Transportation Research Part B 68 (2014) 315–332

Contents lists available at ScienceDirect

Transportation Research Part B

journal homepage: www.elsevier.com/locate/trb

Robust perimeter control design for an urban region

Jack Haddad *, Arie Shraiber

Technion–Israel Institute of Technology, Faculty of Civil and Environmental Engineering, Technion Sustainable Mobility and Robust Transportation (T-SMART) Laboratory, Israel

ARTICLE INFO

Article history:
Received 5 January 2014
Received in revised form 15 May 2014
Accepted 16 June 2014

Keywords:
Macroscopic Fundamental Diagram
Perimeter control
Robust control

ABSTRACT

Recent works have introduced perimeter feedback-control strategies for a homogenous urban region and multiple urban regions with the help of the Macroscopic Fundamental Diagram (MFD) representation, that relates average flow and density (or accumulation) across the network. The perimeter controller is located on the region border, and manipulates the transfer flows across the border, while aiming at regulating around (nearby) the critical densities or accumulations, whereby the system throughput is maximized. While the desired state in the one urban region system is known in advance (given the MFD shape), for the system with multiple urban regions the desired accumulation points are not well known. Moreover, in some traffic scenarios the controller cannot regulate around the critical accumulations for both systems, e.g. because of high demand. In this paper, a robust perimeter controller for an urban region is designed. The controller aims at satisfying the control specifications and having a good performance for the whole accumulation set, uncongested and congested accumulations, and not necessary for a value range nearby the critical accumulation set-point. Moreover, unlike previous works, the robust controller is also designed to handle uncertainty in the MFD and the control constraints within the design level in a systematic way, where the constraints are explicitly integrated utilizing the so-called describing function. Comparison results show that the performances of the robust controller are significantly better than a "standard" feedback controller, for different traffic scenarios.

1. Introduction

Macroscopic Fundamental Diagrams (MFDs) provide aggregate relationships between traffic variables at urban networks. Recently, network traffic flow modeling with the MFD representation has intensively attracted the traffic flow and control researchers, since the MFD simplifies the modelling task of the traffic flow dynamics for large-scale urban networks.

The MFD provides a unimodal, low-scatter relationship between network vehicle density (veh/km) and network space-mean flow or outflow (veh/h) for different network regions, if congestion is roughly homogeneous in the region. Alternatively, the MFD links *accumulation*, defined as the number of vehicles in the region, and *trip completion flow*, defined as the output flow of the region. The physical model of the MFD was initially proposed by Godfrey (1969), but the theoretical elements for the existence of the MFD were provided later by Daganzo (2007). The MFD was first observed with dynamic features in congested urban network in Yokohama by Geroliminis and Daganzo (2008), and investigated using empirical

* Corresponding author. Postal address: Technion City, Rabin Building, Room 726, Israel. Tel.: +972 77 8871742.
E-mail address: jh@technion.ac.il (J. Haddad).

http://dx.doi.org/10.1016/j.trb.2014.06.010
0191-2615/

or simulated data by Buisson and Ladier (2009), Ji et al. (2010), Mazloumian et al. (2010), Daganzo et al. (2011), Zhang et al. (2013), Mahmassani et al. (1987), Olszewski et al. (1995) and others.

Homogeneous networks with small variance of link densities have *a well-defined* MFD (as illustrated in Fig. 1(a)), i.e. low scatter of flows for the same densities (or accumulations) (Geroliminis and Sun, 2011b; Mazloumian et al., 2010; Daganzo et al., 2011; Knoop et al., 2013; Mahmassani et al., 2013. Note that heterogeneous networks might not have a well-defined MFD, mainly in the decreasing part of the MFD, as the scatter becomes higher as accumulation increases and hysteresis phenomena has been found to exist (Daganzo et al., 2011; Buisson and Ladier, 2009; Saberi and Mahmassani, 2012; Geroliminis and Sun, 2011a). As a solution, these networks might be partitioned into more homogeneous regions with small variances of link densities, Ji and Geroliminis (2012). Note that the network topology, the signal timing plans of the signalized intersections, and the infrastructure characteristics affect the shape of the MFD, see e.g. Geroliminis and Boyacı (2012).

The MFD can be utilized to introduce elegant control strategies to improve mobility and decrease delays in large urban networks (Daganzo, 2007; Haddad and Geroliminis, 2012; Geroliminis et al., 2013; Hajiahmadi et al., 2013; Haddad et al., 2013; Aboudolas and Geroliminis, 2013; Keyvan-Ekbatani et al., 2012; Knoop et al., 2012; Zhang et al., 2013. Perimeter control strategies, i.e. manipulating the transfer flows at the perimeter border of the urban region, utilizing the concept of the MFD have been introduced for single-region cities in Daganzo (2007) and Keyvan-Ekbatani et al. (2012), and for multi-region cities in Haddad and Geroliminis (2012), Geroliminis et al. (2013) and Aboudolas and Geroliminis (2013). The Model Predictive Control approach has been used to solve the optimal control problems in Geroliminis et al. (2013), Haddad et al. (2013) and Hajiahmadi et al. (2013), while the classical feedback control approach has been implemented in Keyvan-Ekbatani et al. (2012) and Aboudolas and Geroliminis (2013). The developed MPC solution approach for the different models has performed well for different levels of demand and errors in the MFD's shape, given that the prediction dynamic models are sufficiently accurate. On the other hand, the designed controllers by the classical approach operate according to the feeded information without the need to predict the near-future dynamics or demand, which might be preferable for real practical implementation. Note that the MPC controller does not only integrate feedback information, but its control inputs are also optimal since an objective function is defined explicitly in the control design, while in the classic control approach, the control specification should be defined carefully to obtain optimal desired solutions, which is not a trivial task for different cases. In this paper, we aim at designing a feedback controller following the classical approach.

A Proportional-Integrator (PI) perimeter controller has been designed for an urban region in Keyvan-Ekbatani et al. (2012), while in Aboudolas and Geroliminis (2013) a multivariable feedback regulator for multiple regions has been

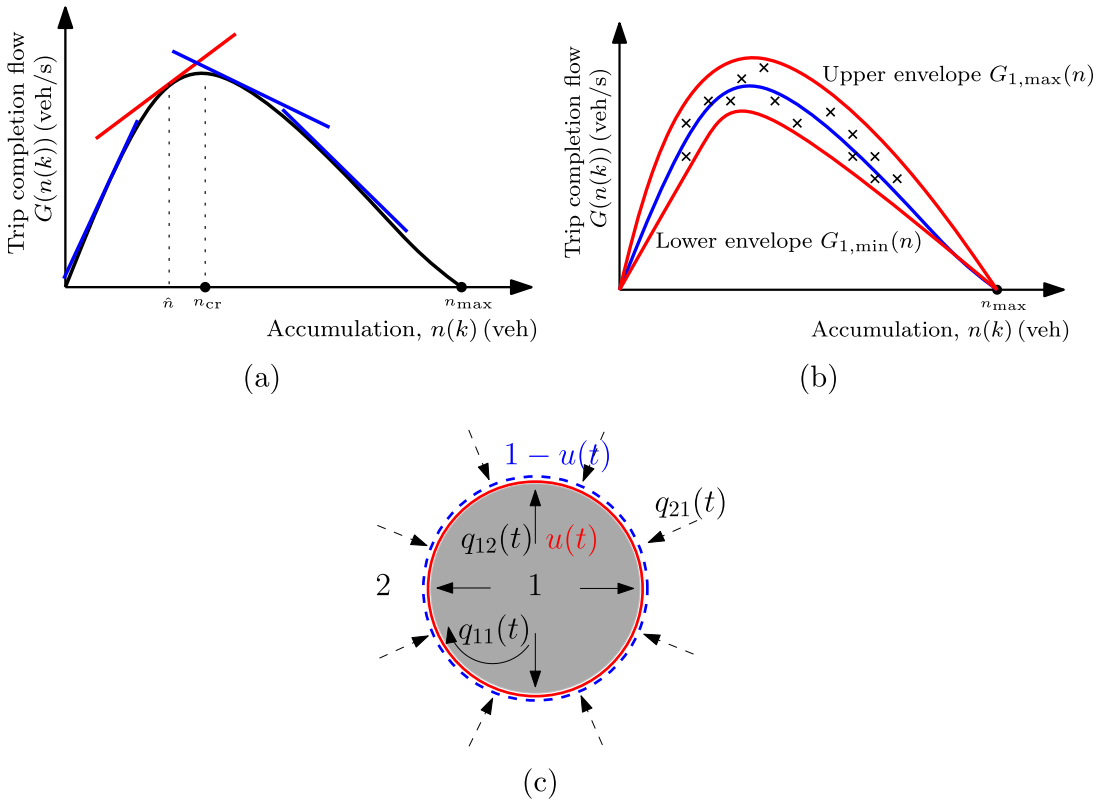

Fig. 1. (a) A well-defined macroscopic fundamental diagram, (b) Upper and lower uncertainty envelopes, (c) An urban region with three traffic demand $q_{11}(t), q_{12}(t), q_{21}(t)$, and a perimeter controller with inputs $u(t)$ and $1-u(t)$.

designed. In both works, the formulated nonlinear systems are linearized around *a priori known* set-point chosen carefully within a value range in the uncongested regime of the MFD having positive slope and close to the critical state of the MFD function, i.e. the critical total time spent in Keyvan-Ekbatani et al. (2012) or the critical accumulations in Aboudolas and Geroliminis (2013). They also aim at regulating the dynamic system around the desired chosen set-point (s), at which the system's throughput is maximized or the system's total time spent is minimized, in other words, the state reference is the same as the set-point. Moreover, both works Keyvan-Ekbatani et al. (2012) and Aboudolas and Geroliminis (2013) do not allow direct consideration of the control constraints, but impose them after the design process, e.g. adjusting or fine-tuning the controller gains.

In this paper, we design a robust perimeter controller for an urban region with the MFD representation. The controller should perform well for the whole state set, and not necessary for a value range nearby a set-point. In fact, we relax ourself in defining in advance the set-point which the nonlinear model is linearized around. Therefore, first the formulated nonlinear model is transformed to a linear model with MFD and parameter uncertainties, where the parameter uncertainty includes all the nonlinearity and the fact that the set-point is not known in advance, and the MFD uncertainty includes the scatter of flows for the same accumulation. Then, we develop a robust controller for the developed uncertainty linear model, i.e. for a given fixed PI-controller with proportional K_P and integrator K_I gains, the controller stabilizes the linear system against all uncertainties. The robust controller is also designed to handle the control constraints within the design level in a systematic way, where the constraints are explicitly integrated utilizing the so-called describing function.

2. Perimeter control model for an urban region

In this paper, a homogeneous urban region that has a well-defined MFD is considered, see black curve in Fig. 1(a). Let $q_{11}(t)$ and $q_{12}(t)$ (veh/s) be the traffic flow demands generated in the region with internal and external destinations, respectively, while $q_{21}(t)$ (veh/s) denotes a generated traffic flow outside the region with destination to the region, as schematically shown in Fig. 1(c). Corresponding to the traffic flow demands, two state variables are used to model the vehicle-conservation equations: $n_{11}(t)$ and $n_{12}(t)$ (veh) are the total number of vehicles in the region with destination to inside and outside the region at time t, respectively. Let us denote $n_1(t)$ as the region accumulation or total number of vehicles in the region at time t, then $n_1(t) = n_{11}(t) + n_{12}(t)$.

The MFD is defined by $G_1(n_1(t))$ (veh/s) which is the trip completion flow for the region at $n_1(t)$. The trip completion flow for the region is the sum of a transfer flow, i.e. trips from the region with external destination (outside the region), plus an internal flow, i.e. trips from the region with internal destination (inside the region). The transfer flow is calculated corresponding to the ratio between accumulations, i.e. $n_{12}(t)/n_1(t) \cdot G_1(n_1(t))$, while the internal flow is calculated by $n_{11}(t)/n_1(t) \cdot G_1(n_1(t))$. These relationships assume that trip length for all trips within a region (internal or external) are similar, i.e. the distance traveled per vehicle inside a region is independent of the origin and destination of the trip. For a description of different cases the reader can refer to Ramezani et al. (2013), which will not alter the methodology. Simulation and empirical results, e.g. in Geroliminis and Daganzo (2008), show that the shape of an MFD can be approximated by a non-symmetric unimodal curve skewed to the right, i.e. critical density that maximizes network flow is smaller than half the jammed density. Thus, we utilize a 3rd-order function of $n_1(t)$, e.g. $G_1(n_1(t)) = a \cdot n_1^3 + b \cdot n_1^2 + c \cdot n_1$, where a, b, c are estimated parameters.

In the control problem, a perimeter control is introduced on the border of the urban region, where its inputs[1] $u(t)$ $(-)$ and $1 - u(t)$ control the ratios of flows, $0 \leqslant u(t) \leqslant 1$, that cross the border from inside to outside and from outside to inside the region at time t, respectively, as shown in Fig. 1(c). It is also assumed that the perimeter control will not change the shape of the MFDs. Note also that the internal flow cannot be controlled or restricted.

Therefore, the vehicle-conservation equations are given as follows

$$\frac{dn_{11}(t)}{dt} = q_{11}(t) + (1 - u(t)) \cdot q_{21}(t) - \frac{n_{11}(t)}{n_1(t)} \cdot G_1(n_1(t)), \tag{1}$$

$$\frac{dn_{12}(t)}{dt} = q_{12}(t) - \frac{n_{12}(t)}{n_1(t)} \cdot G_1(n_1(t)) \cdot u(t). \tag{2}$$

The control problem is defined as follows. Given the dynamic Eqs. (1) and (2), the demands over time $q_{11}(t), q_{12}(t), q_{21}(t)$, and the initial and final (steady-state) accumulations, $n_1(0)$ and $n_{1,ss}$, the control problem aims at manipulating the control input $u(t)$ to bring the initial accumulation $n_1(0)$ to the steady-state accumulation $n_{1,ss}$, while satisfying several specifications, e.g. the solution is stable and the transient period is short (the specifications will be defined later in more details in Section 3.4). Note that if the steady-state accumulation $n_{1,ss}$ is chosen to be the critical accumulation, the control inputs will also maximize the total number of vehicles that complete their trips and reach their destinations, see e.g. in Keyvan-Ekbatani et al. (2012). Note that (1) and (2) are nonlinear equations that do not integrate boundary capacity conditions, which can be taken into account implicitly by defining appropriate lower and upper control bounds. The reader can refer to Haddad et al. (2013) for a different case that the dynamic equations integrate boundary capacity conditions.

[1] Note that in Geroliminis et al. (2013), two different controllers u_{12} and u_{21} are presented on the border. In this paper, we aim at testing our robust controller for a more restrictive and constrained situation, therefore it is assumed that $u_{12} + u_{21} = 1$.

3. Robust perimeter controller design

In this paper, a robust feedback controller is designed in five steps: (1) Deriving steady-state conditions, (2) Deriving a linear parameter-varying (LPV) model, (3) Developing a closed-loop block diagram and its transfer function, with integrated control constraints, (4) Designing robust control parameters, and (5) Integrating input and output disturbances in the closed-loop diagram.

3.1. Deriving necessary conditions for steady-state and transient periods

The feedback controller should be designed such that the control constraint $0 \leqslant u(t) \leqslant 1$ is satisfied during steady-state and transient periods. In the *steady-state period* it holds that the derivatives of the state variables (1) and (2) are equal to zero, i.e. $\mathrm{d}n_{11}/\mathrm{d}t = \mathrm{d}n_{12}/\mathrm{d}t = 0$. Hence, one can isolate the control input in steady-state u_{ss} from (1) and (2) with $\mathrm{d}n_{11}/\mathrm{d}t = \mathrm{d}n_{12}/\mathrm{d}t = 0$, and then derive necessary conditions by satisfying the control constraint $0 \leqslant u_{ss} \leqslant 1$. Let $n_{11,ss}, n_{12,ss}$ (veh) and $q_{11,ss}, q_{12,ss}, q_{21,ss}$ (veh/s) be respectively the state variables and demands at steady-state. Note that the demand in steady-state $q_{11,ss}, q_{12,ss}, q_{21,ss}$ are assumed to be known, while the states $n_{11,ss}$ and $n_{12,ss}$ are calculated from (A.4) and (A.5). For more information, the reader can refer to Appendix A.

We start with the state variable $n_{11}(t)$. Let $\mathrm{d}n_{11}/\mathrm{d}t = 0$ be substituted into (1), one gets at steady-state

$$u_{ss} = \frac{q_{11,ss} + q_{21,ss} - n_{11,ss}/n_{1,ss} \cdot G_1(n_{1,ss})}{q_{21,ss}}. \tag{3}$$

Since u_{ss} should satisfy the constraints $0 \leqslant u_{ss}$ and $u_{ss} \leqslant 1$, one respectively gets the following necessary conditions

$$G_1(n_{1,ss}) \leqslant q_{11,ss} + q_{21,ss}, \tag{4}$$

$$q_{11,ss} \leqslant \frac{n_{11,ss}}{n_{1,ss}} \cdot G_1(n_{1,ss}). \tag{5}$$

Similar derivation is done for the state variable $n_{12}(t)$. One can isolate u_{ss} in (2) with $\mathrm{d}n_{12}/\mathrm{d}t = 0$ as follows

$$u_{ss} = \frac{q_{12,ss} \cdot n_{1,ss}}{G_1(n_{1,ss}) \cdot n_{12,ss}}, \tag{6}$$

and the obtained necessary conditions satisfying $0 \leqslant u_{ss}$ and $u_{ss} \leqslant 1$ are, respectively,

$$0 \leqslant q_{12,ss} \cdot n_{1,ss}, \tag{7}$$

$$q_{12,ss} \leqslant \frac{n_{12,ss}}{n_{1,ss}} \cdot G_1(n_{1,ss}). \tag{8}$$

Note that the condition (7) always holds, since the steady-state state $n_{1,ss}$ and demand $q_{12,ss}$ are clearly assumed to be non-negative. Hence, the necessary conditions (4), (5), and (8) must hold in steady-state to satisfy the control constraint.

In the same way, necessary conditions are derived for the *transient period*, i.e. the time period in which the initial accumulation is being brought to the steady-state accumulation. In order to increase or decrease the initial accumulation to the steady-state accumulation, the condition $\mathrm{d}n_1/\mathrm{d}t > 0$ or $\mathrm{d}n_1/\mathrm{d}t < 0$ should be satisfied, respectively, satisfying the control constraint $0 \leqslant u(t) \leqslant 1$. Note that $\mathrm{d}n_1/\mathrm{d}t$ is obtained by summing (1) and (2). Therefore, one gets the following necessary conditions for the transient period

$$G_1(n_1(t)) > q_{11}(t) + q_{12}(t), \tag{9}$$

$$G_1(n_1(t)) < q_{11}(t) + q_{12}(t) + q_{21}(t). \tag{10}$$

3.2. Deriving a control design LPV-model

We simplify the nonlinear system model (1) and (2) by deriving a linear model with parametric uncertainty, whereas the uncertainty should capture the nonlinearity dynamics. Hence, we first define a parameter $\alpha(t)$ $(-)$ as $\alpha(t) = n_{11}(t)/n_1(t)$ and rewrite $n_{12}(t)/n_1(t) = 1 - \alpha(t)$, then we sum (1) and (2), one gets

$$\frac{\mathrm{d}n_1(t)}{\mathrm{d}t} = q_{11}(t) + q_{12}(t) + (1 - u(t)) \cdot q_{21}(t) - \alpha(t) \cdot G_1(n_1(t)) - (1 - \alpha(t)) \cdot G_1(n_1(t)) \cdot u(t). \tag{11}$$

Note that (11) is a nonlinear equation that depends only on one state variable $n_1(t)$, but has a parameter $0 \leqslant \alpha(t) \leqslant 1$. Let us now assume that the MFD function $G_1(\cdot)$ is not well-defined and has some uncertainty in the value of the trip completion flow. We assume that the uncertain MFD is another function, denoted by $\widetilde{G}_1(\cdot)$, that can vary between lower and upper envelopes of the MFD with uncertainty, denoted respectively by $G_{1,\min}(\cdot)$ and $G_{1,\max}(\cdot)$, see Fig. 1(b). Let us now linearize the nonlinear system model (11) around a set-point $(\hat{n}_1, \hat{u})$, one gets the following linear parameter-varying (LPV) model

$$\frac{d\Delta n_1(t)}{dt} = A(\alpha, \widetilde{G}_1) \cdot \Delta n_1(t) + B(\alpha, \widetilde{G}_1) \cdot \Delta u(t), \tag{12}$$

where $\Delta n_1(t) = n_1(t) - \hat{n}_1$ and $\Delta u(t) = u(t) - \hat{u}$, and

$$A(\alpha, \widetilde{G}_1) = -\frac{d\widetilde{G}_1(\hat{n}_1)}{dn_1} \cdot (\alpha + (1-\alpha) \cdot \hat{u}), \tag{13}$$

$$B(\alpha, \widetilde{G}_1) = -q_{21,ss} - (1-\alpha) \cdot \widetilde{G}_1(\hat{n}_1). \tag{14}$$

The LPV model (12)–(14) with uncertain parameter α and uncertain MFD $\widetilde{G}_1(\cdot)$ approximates the original nonlinear system (1) and (2) near the set-point $(\hat{n}_1, \hat{u})$. Note that input and output disturbances are considered later in SubSection 3.5. In the following, we design a robust controller that stabilizes the system against all uncertainty in α and $\widetilde{G}_1(\cdot)$.

3.3. Developing a closed-loop block diagram and its transfer function

We develop the closed-loop block diagram and transfer function as follows. First, we apply Laplace transformation to the control design model (12), which is transformed to the frequency domain as follows

$$\Delta N_1(s) = \frac{B(\alpha, \widetilde{G}_1)}{s - A(\alpha, \widetilde{G}_1)} \cdot \Delta U(s). \tag{15}$$

Similar to Keyvan-Ekbatani et al. (2012) and Aboudolas and Geroliminis (2013), we design a PI-controller with proportional K_P gain and integral K_I gain, which is $K_P + \frac{K_I}{s}$. We integrate the control constraint $0 \leqslant u \leqslant 1$ in the loop with the help of a describing function, refer to Gelb and Velde (1968), that is modeled by uncertain gain $\widetilde{P}$ in the frequency domain having the range of values $[\widetilde{P}_{min}, \widetilde{P}_{max}] = [1/u_{amp}, 1]$, where u_{amp} is the coefficient of the first Fourier transformation for a saturation function. Finally, we close the loop with the reference $\Delta N_{1,ss}$ as shown in Fig. 2. Note that $\Delta n_{1,ss}(t) = n_{1,ss}(t) - \hat{n}_1$ and $\Delta n_1(t) = n_1(t) - \hat{n}_1$. Corresponding to the block diagram (without input and output disturbances, i.e. $D_{in} = D_{out} = 0$) in Fig. 2, the closed-loop transfer function is calculated as follows

$$\mathcal{CL}_{\Delta N_{1,ss}, \Delta N_1} = \frac{K_P \widetilde{P} B s + K_I \widetilde{P} B}{s^2 + (K_P \widetilde{P} B - A)s + K_I \widetilde{P} B}. \tag{16}$$

3.4. Designing robust control parameters

The robust PI (R-PI) controller gains are designed, following the Quantitative Feedback Control (QFT) theory concepts, see Houpis et al. (2006), according to the following closed-loop control specifications: (S1) the closed-loop transfer function $\mathcal{CL}_{\Delta N_{1,ss}, \Delta N_1}$ must be stable, and (S2) should have exponential step response, i.e. two real poles (or no complex roots), while the control initial and steady-state inputs have to satisfy (S3) the initial value theorem and (S4) the final value theorem. These specifications should hold against all uncertainties in α and $\widetilde{G}_1$. The physical meaning from the control specifications are as follows: S1 guaranties that the control inputs will bring the initial accumulation to the steady-state accumulation for all cases and under all uncertainties, while S2 guaranties that the accumulation will not have an overshoot during the transient period, and S3 and S4 guaranty to integrate the control constraints during the transient and steady-state periods.

First, we calculate the minimum and maximum bounds of $A(\alpha, \widetilde{G}_1)$ and $B(\alpha, \widetilde{G}_1)$, in order to design the gain parameters K_P and K_I for the worst case combination. Designing for the worst case combination aims at covering all possible uncertainties, which results in designing the dynamic system (12) for all possible set-points. The bounds of $A(\alpha, \widetilde{G}_1)$ and $B(\alpha, \widetilde{G}_1)$ are calculated from (13) and (14) with the constraint that $0 \leqslant \alpha \leqslant 1$, and $\widetilde{G}_1(\hat{n}_1) \in [G_{1,min}(\hat{n}_1), G_{1,max}(\hat{n}_1)]$ as follows

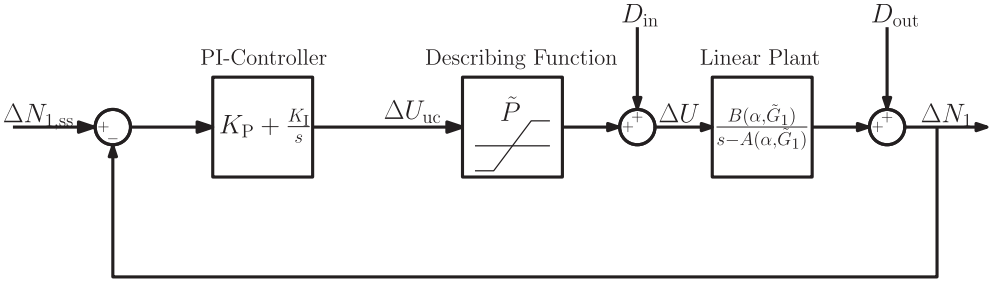

Fig. 2. A closed-loop block diagram for an urban region system.

$$A_{\min} = -2 \cdot \max_{\widetilde{G}_1} \left. \frac{d\widetilde{G}_1(\hat{n}_1)}{dn_1} \right|_{\hat{n}_1 = \operatorname{argmax} d\widetilde{G}_1(\hat{n}_1)/dn_1}, \tag{17}$$

$$A_{\max} = -2 \cdot \min_{\widetilde{G}_1} \left. \frac{d\widetilde{G}_1(\hat{n}_1)}{dn_1} \right|_{\hat{n}_1 = \operatorname{argmin} d\widetilde{G}_1(\hat{n}_1)/dn_1}, \tag{18}$$

$$B_{\min} = -q_{21} - \max_{\widetilde{G}_1} \left. \widetilde{G}_1(\hat{n}_1) \right|_{\hat{n}_1 = \operatorname{argmax} \widetilde{G}_1(\hat{n}_1)}, \tag{19}$$

$$B_{\max} = -q_{21}. \tag{20}$$

Note that $A_{\min} < 0 < A_{\max}$ and $B_{\min} < B_{\max} < 0$.

Stability of the closed-loop function $\mathcal{CL}_{\Delta N_{1,ss},\Delta N_1}$ is determined by its poles $\lambda_i, i = 1, 2$, or simply the roots of the denominator equation in (16), i.e.

$$\lambda_{1,2} = \frac{-(K_P \widetilde{P} B - A) \pm \sqrt{(K_P \widetilde{P} B - A)^2 - 4 K_I \widetilde{P} B}}{2}. \tag{21}$$

For stability, the real part of every pole must be negative, i.e. $\Re(\lambda_{1,2}) < 0$. Therefore, S1 is satisfied if

$$K_P < \frac{A}{\widetilde{P} B}, \tag{22}$$

$$K_I > \frac{(K_P \widetilde{P} B - A)^2}{4 \widetilde{P} B}. \tag{23}$$

Note that K_I and K_P are negative. Given (17)–(20), the K_I and K_P parameters for the worst case combination of A and B within their lower and upper bounds should satisfy

$$K_P \leqslant \frac{\phi A_{\max}}{\widetilde{P}_{\min} B_{\min}}, \tag{24}$$

$$K_I \geqslant \frac{(\phi - 1) A_{\max}}{4 \widetilde{P}_{\max} B_{\max}}, \tag{25}$$

where ϕ $(-)$ and $\phi - 1, \phi > 1$, are multiplied in (24) and (25), respectively, to assure that the transformation from the *strict* inequality in (22) and (23) to *not strict* inequality in (24) and (25) holds.

The closed-loop specification S2 holds since the discriminant of (21) will not have complex roots as it is always positive for K_P and K_I in (24) and (25), i.e. $(K_P \widetilde{P} B - A)^2 - 4 K_I \widetilde{P} B > 0$.

To utilize the initial and final value theorems, we calculate the transfer function from $\Delta U(s)$ to $\Delta N_{1,ss}(s)$, see Fig. 2,

$$\Delta U(s) = \mathcal{CL}_{\Delta N_{1,ss},\Delta N_1} \cdot \frac{s - A}{B} \cdot \Delta N_{1,ss}(s). \tag{26}$$

The control inputs to the plant should be bounded in $[0, 1]$ during the transient and steady-state periods. This can be respectively satisfied with the help of the initial and final value theorems as follows. To satisfy the control constraint during the transient process, the unconstrained control inputs $\Delta u_{uc}(t)$ to the saturation function, see Fig. 2, should satisfy $\Delta u_{uc}(t) < \pi u_{amp}$, where πu_{amp} is the approximation of the maximum input value to the saturation function.[2] From S2, the dynamic system will have an exponential step response, hence, satisfying the constraint for the initial control input $\Delta u_{uc}(0)$, which is the highest possible value, implies that the control constraint $0 \leqslant u(t) \leqslant 1$ holds for the whole transient period. Hence, applying the initial value theorem (S3), $\Delta u(0) = \lim_{s \to \infty} s \Delta U(s)$, one gets

$$K_P \leqslant -\frac{\pi u_{amp}}{|n_{1,ss} - n_1(0)|}. \tag{27}$$

Therefore, K_P is determined by (24) and (27). Moreover, the control input in steady-state should also be bounded. Utilizing the final value theorem, $\Delta u(\infty) = \lim_{s \to 0} s \Delta U(s)$, one has to satisfy the following condition

$$\Delta n_{1,ss} = n_{1,ss} - \hat{n}_1 \leqslant \left| \frac{B_{\min}}{A_{\max}} \right|. \tag{28}$$

[2] Numerical tests show that the control inputs $\Delta u_{uc}(t)$ follow a decreasing exponential behaviour, that can be approximated by a triangular shape, and the coefficient of the first Fourier transformation of the triangular shape for the saturation function is πu_{amp}.

Note that this condition relates the maximum difference value between the steady-state accumulation and the arbitrary chosen set-point.

3.5. Integrating input and output disturbances

In previous subsections, the input disturbance D_{in} and the output disturbance D_{out} have not been considered in the closed-loop diagram shown in Fig. 2, as they are assumed to be $D_{in}(t) = D_{out}(t) = 0$. In this subsection, input and output disturbances are integrated in the closed-loop diagram to analyze the R-PI controller rejection, inter alia, for estimation errors in accumulation (see also numerical example 5 in Section 4).

Considering the disturbances in the closed-loop diagram shown in Fig. 2, one can calculate the output ΔN_1 as a function of the state reference $\Delta N_{1,ss}$ and the input and output disturbances, D_{in} and D_{out}, as follows

$$\Delta N_1 = \mathcal{CL}_{\Delta N_{1,ss},\Delta N_1} \cdot \Delta N_{1,ss} + \mathcal{CL}_{D_{in},\Delta N_1} \cdot D_{in} + \mathcal{CL}_{D_{out},\Delta N_1} \cdot D_{out}, \tag{29}$$

where $\mathcal{CL}_{D_{in},\Delta N_1}$ and $\mathcal{CL}_{D_{out},\Delta N_1}$ are respectively the closed loop transfer functions from input and output disturbances to output, and calculated as follows

$$\mathcal{CL}_{D_{in},\Delta N_1} = \frac{sB}{s^2 + (K_P\widetilde{P}B - A)s + K_I\widetilde{P}B}, \tag{30}$$

$$\mathcal{CL}_{D_{out},\Delta N_1} = \frac{s(s - A)}{s^2 + (K_P\widetilde{P}B - A)s + K_I\widetilde{P}B}. \tag{31}$$

For more information, the reader can refer to Appendix B. Clearly, the denominator of the transfer functions $\mathcal{CL}_{\Delta N_{1,ss},\Delta N_1}, \mathcal{CL}_{D_{in},\Delta N_1}, \mathcal{CL}_{D_{out},\Delta N_1}$, see respectively (16), (30), (31), is the same, i.e. $s^2 + (K_P\widetilde{P}B - A)s + K_I\widetilde{P}B$, which its stable poles are already calculated in (21). Recall that the closed-loop control specifications (S1)–(S4), inter alia the stability specification, have been earlier satisfied for this denominator by designing the gains K_I and K_P accordingly, see (24) and (25). Therefore, if biased and/or unbiased errors in output and/or input exist, the controller will still stabilize the accumulation towards the desired accumulation and all other specifications should also hold, as long as steady-state and transient necessary conditions *with disturbance (s)* hold. Note that the steady-state necessary conditions (4), (5), (8) and the transient necessary conditions (9) and (10) have been derived *without* taking into account the disturbances, i.e. assuming $D_{in}(t) = D_{out}(t) = 0$. Deriving necessary conditions with disturbance (s), by satisfying the control constraint $0 \leqslant u_{ss} \leqslant 1$, is not a trivial task for the nonlinear system (1) and (2). However, since the LPV-model (12) approximates the nonlinear model (1) and (2), utilizing the LPV-model makes the task easier. The transfer function from the disturbance (s) to Δu_{uc} should be first derived. Then, utilizing the initial and final theorems and imposing the control constraints, one can derive necessary conditions with disturbance(s).

In the following, we derive a steady-state necessary condition taking into account only the output disturbance D_{out}, i.e. $D_{in}(t) = 0$. The output disturbance can model errors in regional accumulation. The unconstrained control input ΔU_{uc} can be calculated as a function of the disturbance D_{out}, as follows

$$\Delta U_{uc} = \mathcal{CL}_{D_{out},\Delta U_{uc}} \cdot D_{out}, \tag{32}$$

where $\mathcal{CL}_{D_{out},\Delta U_{uc}}$ is the transfer function from disturbance D_{out} to ΔU_{uc}, i.e.

$$\mathcal{CL}_{D_{out},\Delta U_{uc}} = \frac{K_P s^2 + (K_I - AK_P)s - AK_I}{s^2 + (K_P\widetilde{P}B - A)s + K_I\widetilde{P}B}. \tag{33}$$

Applying the final value theorem, $\Delta u_{uc}(\infty) = \lim_{s\to 0} s\Delta U_{uc}(s)$, and assuming a step disturbance with a size of $d_{out,max}$ (veh), then the control constraint will be satisfied if the following necessary condition holds

$$-u_{ss} \leqslant \Delta u_{uc} = \frac{-Ad_{out}}{\widetilde{P}B} \leq 1 - u_{ss}. \tag{34}$$

Note that form (34) one can calculate the maximum size of the step disturbance, d_{out}, to which the R-PI controller can still reject. In the next section, numerical examples demonstrate and analyze the R-PI controller's rejection against biased and unbiased errors in accumulation and MFD.

4. Case study examples

In this section, results of several case study examples are presented to explore the features of the robust PI (R-PI) controller, see (24), (25), and (27), under different traffic conditions. The examples aim at examining the efficiency of the R-PI controller in uncongested and congested regimes which may vary with time, e.g. because of variations in demand. A comparison with a "standard" PI (S-PI) controller is carried out, as we compare the results obtained from applying the S-PI and R-PI controllers for the original nonlinear plant (11) and the linear plant (12).

In the following Examples 1–3, we assume a well-defined MFD without uncertainty, i.e. $G_1(\cdot) \equiv \widetilde{G}_1(\cdot) \equiv G_{1,min}(\cdot) \equiv G_{1,max}(\cdot)$. The MFD for the urban region is $G_1(n_1) = (1.4877 \cdot 10^{-7} n_1^3 - 2.9815 \cdot 10^{-3} n_1^2 + 15.0912 n_1)/3600$, with

$n_{1,cr} = 3400(\text{veh}), G_1(n_{1,cr}) = 6.3(\text{veh/s})$, and $n_{1,jam} = 10000(\text{veh})$. This shape is consistent with the MFD observed in Yokohama. While in Example 4, we investigate the effect of uncertainty in MFDs on the R-PI controllers, therefore, another three MFDs are introduced, as explained below and as shown in Fig. 9. Note that the uncertainty in α is considered for all examples.

4.1. Designing S-PI and R-PI controllers

Both S-PI and R-PI controllers are designed according to the corresponding linear plants. The R-PI controller is designed for all possible linear plants with the help of the LPV model in (12), with $u_{amp} = 100$ or $\widetilde{P}_{min} = 0.01$ and $\widetilde{P}_{max} = 1$, while the S-PI controller is designed for one specific plant defined by $\widehat{A}$ and $\widehat{B}$, which are calculated from $A(\alpha, \widetilde{G}_1)$ and $B(\alpha, \widetilde{G}_1)$ in (13) and (14), respectively, at a given set-point $\hat{n}_1$. We choose the set-point $\hat{n}_1 = 3060$ (90% of $n_{1,cr}$), and the calculated parameters are $\widehat{A} = -3.74 \cdot 10^{-4}$ and $\widehat{B} = -9.28$.

Note that the S-PI controller is designed carefully satisfying the same specifications defined for the R-PI controller in Section 3.4, and summarized as follows: (i) the closed-loop is stable and has exponential step response, and (ii) the control inputs are bounded. With these specifications, we assure a fair comparison with our proposed R-PI controller in the next section. Therefore, we first aim at satisfying the control constraint for the initial input following the initial value theorem. The proportional gain K_P is calculated from (27) with maximum difference between initial and final accumulations $|n_{1,ss} - n_1(0)| = 1000(\text{veh})$, given that the controller operates within a region set $2400 - 3400(\text{veh})$. Now, in order to satisfy the exponential closed-loop step response to guaranty fast regulating around the accumulation reference without oscillation behaviour over the accumulation reference, one can calculate K_I from equalising the discriminant of (21) to zero. The calculated gains for the S-PI controller are $K_P = -0.1$ and $K_I = -2.14 \cdot 10^{-5}$. Note that these gains satisfy the final theorem condition, therefore, the control constraint in steady-state also holds.

4.2. Numerical results

In Example 1, we compare between the S-PI and R-PI controllers while the system is operated within the uncongested regime of the MFD, in a region of $2400 - 3400(\text{veh})$ nearby the set-point $\hat{n}_1 = 3060$ (veh) to which the system dynamics is linearized around. We choose to regulate around the set-point, i.e. the reference or steady-state accumulation and the set-point accumulation are the same $\hat{n}_1 = n_{1,ss}$. The given constant demand ($q_{11} = 0.75, q_{12} = 1.5, q_{21} = 5$ (veh/s)) simulate a morning peak hour with high demand q_{21} for trips outside towards inside the region, i.e. from the periphery to the city center, and the initial accumulation is $n_1(0) = 2400$ (veh).

The accumulation and control input results of the S-PI and R-PI controllers applied to linear and nonlinear plants are shown in Fig. 3. It is shown that the two controllers have similar performance while applied to both the linear and nonlinear plants, see coincide accumulation curves in the figure. Both controllers reach the accumulation reference having a small steady-state error, and the control inputs are within the lower and upper bounds. It is shown that the R-PI controller has no advantage compared with the S-PI controller for this case. This is correct, since the linearized model around the set-point in this region is very close to the nonlinear model (the MFD function in the uncongested part is almost linear, and the slope at the set-point is close to the slope of the MFD function), hence, the nonlinearity of the model does not affect the results. The obtained gains of the R-PI and S-PI controllers are the same and determined by the same critical specification (initial value theorem or (27)).

In numerical example 2, we investigate two cases where the initial and final accumulation values are far from the set-point region. In case (2a) the urban region is initially congested, i.e. the initial accumulation $n_1(0) = 7000$ (veh) is in

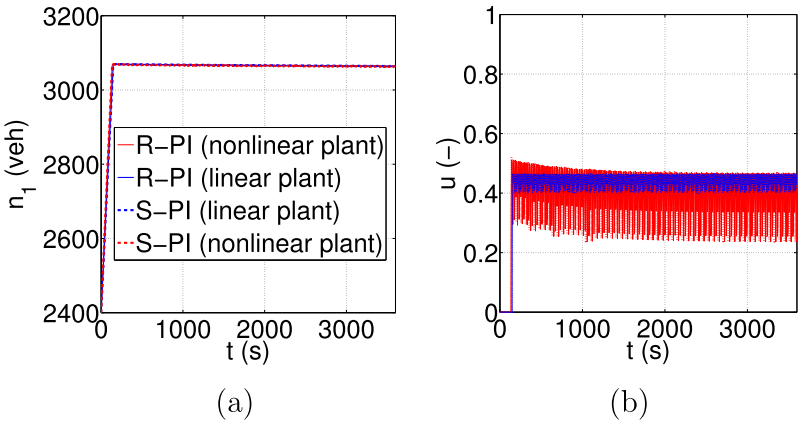

Fig. 3. Example 1: Operating within a region (2400–3400 (veh)) nearby a set-point ($\hat{n}_1 = 3060$ (veh)). Linear and original nonlinear plants with R-PI and S-PI controllers: (a) accumulation and (b) control input.

the decreasing part of the MFD, which means that the region operates close to capacity conditions. The accumulation reference is set to be in the increasing part of the MFD, i.e. $n_{1,ss} = 1000$ (veh). Case (2b) is the vice versa with $n_1(0) = 1000$ (veh) and $n_{1,ss} = 7000$ (veh). The evolution of accumulations over time $n_1(t), 0 \leqslant t \leqslant 3600$ (s), corresponding to the S-PI controller, applied to linear (blue curve) and nonlinear (red curve) plants, for cases (2a) and (2b) are presented in Fig. 4(a) and (b), respectively, while the accumulation evolution presented in Fig. 4(c) and (d) are respectively corresponding the R-PI controller. The comparison results show that if the initial accumulation $n_1(0)$ and the steady-state accumulation (or reference) $n_{1,ss}$ are far from each other, see (27), the R-PI controller is superior for the two cases presented, as it brings both initial accumulations to the accumulation reference with small steady-state errors as shown in Fig. 4(c) and (d), while the S-PI has poor performances as the accumulation in steady-state does not converge to the reference, see Fig. 4(b), or it takes a long time to be close to it as shown in Fig. 4(a).

Example 2 is further utilized to investigate the R-PI controller performances by comparing it with an MPC controller. The MPC controller determines the optimal control inputs in a receding horizon manner, where at each time step an objective function is optimized for a prediction horizon, then only the first control input is applied to the plant (reality). This procedure is carried out again with a shifted horizon until the whole control process time is covered. For more information about MPC applications to perimeter control with MFD dynamics, the reader can refer to Geroliminis et al. (2013) and Haddad et al. (2013), while theoretical issues of MPC can be found in, e.g., Camacho and Bordons (1999).

The control inputs of the MPC controller are obtained by minimizing an objective function J over the prediction horizon $[0, t_f]$, with the nonlinear dynamic model (1) and (2) and subject to the control constraint $0 \leqslant u(t) \leqslant 1$. The objective function J is defined as the time integral of the square of the difference between the state and the reference state, i.e. $J = \int_0^{t_f} (n_1(t) - n_{1,ss})^2 dt$. The objective function J of the MPC controller aims at reaching the reference accumulation similarly to the R-PI controller, which results in a fair performance comparison between the results of both controllers.

The accumulation results over time corresponding to the MPC controller applied to the nonlinear plant, for cases (2a) and (2b) are respectively presented in Fig. 4(c) and (d). The accumulation results show that the R-PI and MPC controllers have similar performance. This claim is supported by other numerical examples that have been tested but not reported in this paper. Although similar accumulation results are obtained by applying MPC and R-PI controllers, the obtained control input

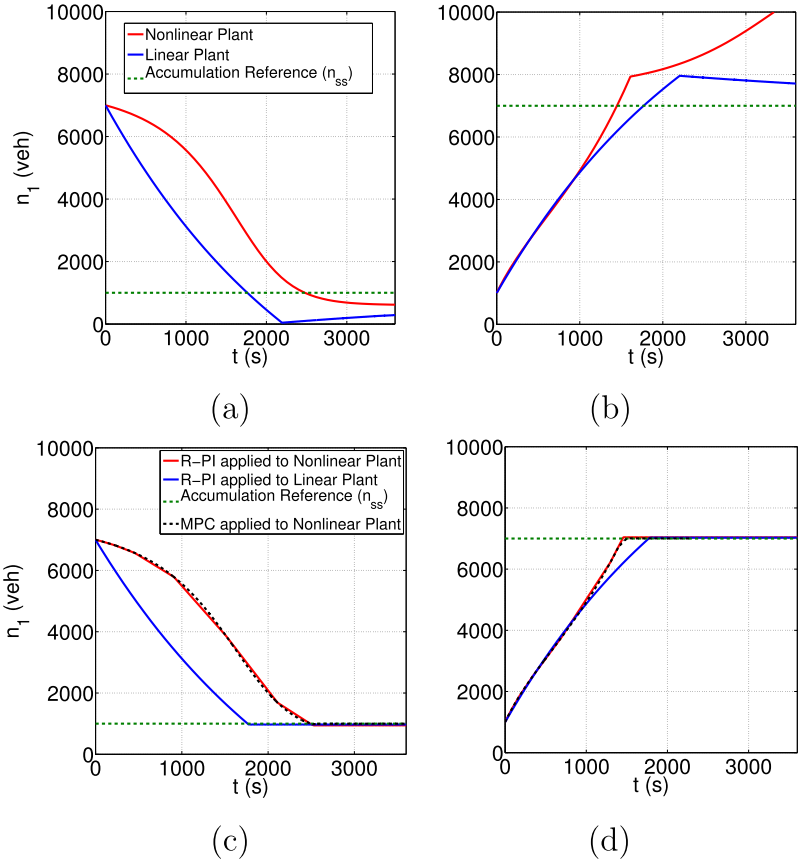

Fig. 4. Example 2: Obtained accumulations by applying S-PI and R-PI controllers to linear (blue curve) and nonlinear (red curve) plants, from initially-congested accumulation to finally-uncongested accumulation in (a) and (c), respectively, and vice versa in (b) and (d). The results of the MPC controller applied to the nonlinear plant are also shown in (c) and (d). (For interpretation of the references to colour in this figure legend, the reader is referred to the web version of this article.)

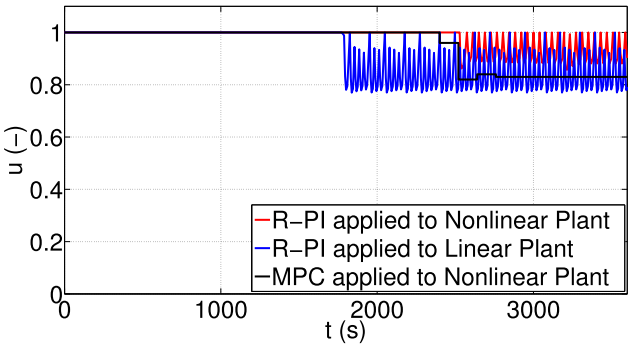

Fig. 5. Example 2: Comparison between control sequences obtained by the R-PI and MPC controllers.

sequence profiles are not similar, as shown in Fig. 5 for case (2a), i.e. initially-congested accumulation $n_1(0) = 5000$ (veh). The latter results show that the control input *profiles* for both controllers are different mainly in the steady-state period. Since the R-PI controller is a regulator feedback controller, its control input sequence has a chattering behaviour, while the control input sequence of the MPC during the steady-state period is constant. This might be considered as an advantage of the MPC controller over the R-PI controller, since less control efforts are needed. On the other hand, one should notice that the computational complexity of the MPC controller is much higher than the R-PI controller, as at each time step an open-loop optimization problem for the prediction horizon is solved. Moreover, note that the MPC controller has number of parameters that should be tuned, e.g. the prediction horizon length. Such a parameter should be carefully chosen only after many simulation runs, and should be also tuned if the model parameters change in the future, while the R-PI controller is designed for a fixed controller with K_I and K_P against all uncertainty in the model.

In Example 2, we also examine and demonstrate the effect of violating (at least one of) the transient necessary conditions (9) and (10). Fig. 6 shows the results for Example 2 case (2a) with initial accumulation of $n(0) = 8000$ (veh) (instead of 7000). It is shown that the R-PI controller applied to the linear plant works well, as it brings the initial accumulation to the steady-state accumulation, while the accumulation diverges by applying the R-PI controller to the nonlinear plant. Even though the steady-state conditions (4), (5), and (8) hold, the accumulation does not reach the steady-state accumulation since the transient necessary conditions (9) and (10) do not hold at the initial accumulation (and afterwards). Note that similar diverge results are obtained for initial accumulations that are larger than 7500 (veh), $n_1(0) > 7500$. The reason for that is the existence of a bifurcation (unstable) equilibrium point at ≈ 7500 (veh), where all initial accumulations larger than 7500 are within an unstable state region that go to gridlock, and there does not exist any control input that can prevent that (unless the demand decreases in the future). For more information regarding the stability analysis of perimeter control for an urban network with MFD representation, the reader can refer to Haddad and Geroliminis (2012). The results in Fig. 6 (Example 2, case (2a), with $n(0) = 8000$) show that violating (at least one of) the transient necessary conditions (9) and (10), derived from *the nonlinear model*, results in poor performance of the designed controller applied to the nonlinear plant. Note that for other numerical examples, e.g. $n_1(0) = 7000, n_{1,ss} = 1000$, and $\hat{n}_1 = 6000$, we cannot even success in designing an R-PI controller, since the steady-state necessary condition (28), derived from *the linear model*, cannot be satisfied. This demonstrates the importance of considering both the linear and nonlinear dynamic systems in the control design and analysis.

Moreover, the performance of the R-PI controller is numerically investigated for different levels of demand for case (2a) in Example 2. Consider the base case with $q_{11} = 0.75, q_{12} = 1.5, q_{21} = 5$ (veh/s). Results in Fig. 7(a)-(c), show respectively the effect of different levels of q_{11} (=0.25, 0.5, 0.75, 1, 1.25), q_{12} (=1, 1.25, 1.5, 1.75, 2.0), and q_{21} (=4.5, 4.75, 5.0, 5.25, 5.5) in the accumulation response over time. It is shown that increasing or decreasing the demand q_{11} and q_{12} with respect to the base case, i.e. the red curves in Fig. 7(a) and (b), has the same effect on the accumulation response. This holds since both q_{11} and q_{12} are free elements in the right hand side of the dynamic accumulation Eq. (11). On the other hand, increasing or decreasing the demand q_{21} within the tested values does not affect the accumulation response over time as shown in Fig. 7(c). This holds since the urban region is initially congested and operates close to capacity conditions, where the control inputs will be close to its upper limit value preventing vehicles from outside to enter the congested region. Hence, increasing or decreasing q_{21} does not have any more effect on the accumulation dynamics, and accumulation response curves coincide in this case. This is also in compliance with (11) as $u \to 1$, the $(1-u)\cdot q_{21} \to 0$. Note that in other cases, increasing or decreasing the demand q_{21} can affect the accumulation response, but they will have the same trend, i.e. the accumulation curves will converge to an upper curve while increasing the demand as the control input reaches its upper limit.

In numerical example 3, we show that the designed R-PI controller operates very well for any chosen set-point. Unlike the S-PI controller that is designed for a priori known set-point, there is no need to know in advance the set-point for the R-PI controller as it is designed for all possible points. Recall that the R-PI controller is already tested for the moderate-congested set-point $\hat{n}_1 = 3060$ (veh) in Example 1, see Fig. 3. In Fig. 8, the R-PI controller is tested for (a) an uncongested set-point $\hat{n}_1 = 2000$ (veh), and for (b) a congested set-point $\hat{n}_1 = 5000$ (veh), where the steady-state and set-point accumulations are equal, i.e. $n_{1,ss} = \hat{n}_1$, and the initial accumulation is $n_1(0) = 3060$ (veh). Note that regulating around a set-point which

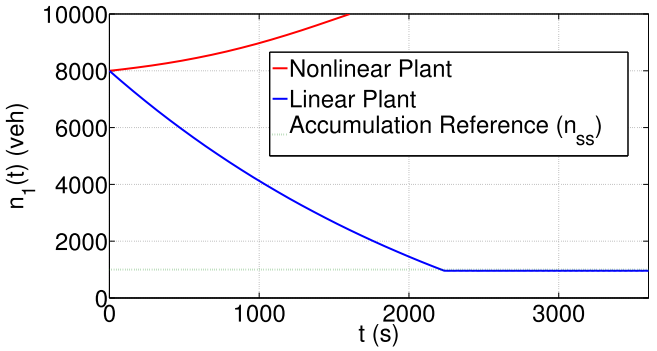

Fig. 6. Example 2: the R-PI controller is applied to linear and nonlinear plants.

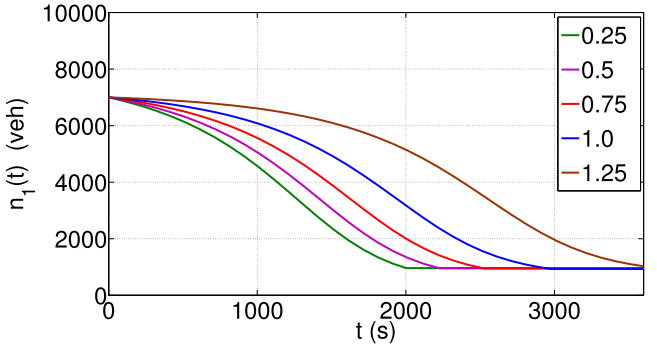

(a)

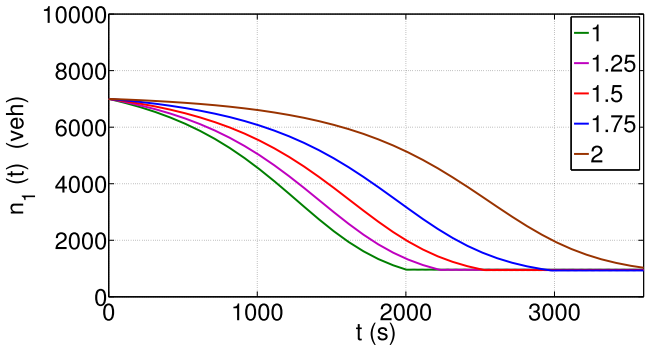

(b)

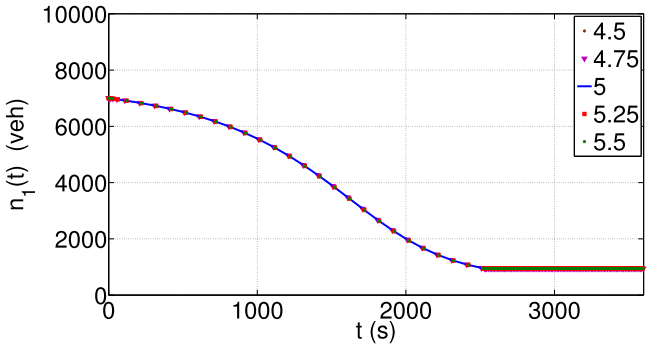

(c)

Fig. 7. Example 2: different levels of demand: (a) $q_{11} = 0.25, 0.5, 0.75, 1, 1.25$ (veh/s), (b) $q_{12} = 1, 1.25, 1.5, 1.75, 2.0$ (veh/s), and (c) $q_{21} = 4.5, 4.75, 5.0, 5.25, 5.5$ (veh/s).

is not the moderate-congested point, i.e. an uncongested or a congested set-point, is an important task when the steady-state state cannot be reached for moderate-congestion because of low or high demand. This is also crucial for multi-region systems, since some of the regions will be more congested than others, and the controller cannot regulate all regions at their moderate-congestion accumulations. The results in Fig. 8 show that the R-PI controller has a better performance as it regulates around the steady-state (or reference) accumulation very fast, while the S-PI controller has accumulation overshoots, i.e. the accumulation goes below 2000 (veh) in case (2a), and above 5000 in case (2b). This happens since the S-PI controller is designed for a linearized system around $\hat{n}_1 = 3060$ (veh). The overshoot response behaviour results in further delays, which can be eliminated or decreased by redesigning the S-PI controller to the appropriate set-point. In fact, since the two controllers are PI controllers, the S-PI controller can be fine-tuned to have similar performance to the R-PI controller.

In numerical example 4, two further issues are examined: (i) testing the control design of R-PI controllers for *different* well-defined MFDs, and (ii) evaluating the performance of an R-PI controller under MFD uncertainty. Hence, in order to test these issues, another three MFDs are obtained based on deviation from the critical accumulation n_{cr} and the maximum trip completion flow $G_1(n_{cr})$ of the Yokohama MFD. The percentages of the deviations are $-5\%, +5\%$, and $+20\%$ for both the critical accumulation and the maximum trip completion flow as shown in Fig. 9.

The control design is tested by examining the performance of R-PI controllers designed according to different well-defined MFDs (without uncertainty), i.e. the R-PI controller is designed according to an MFD, and it is assumed that the reality or plant has the *same* MFD. The accumulation responses to R-PI controllers designed according to different well-defined MFDs are shown in Fig. 10. The figure shows that the R-PI controllers work well satisfying the control specifications for different MFDs. Note that in the figure, results are shown only for $\pm 5\%$ variations, but good performance is also guaranteed for higher percentages as long as the steady-state conditions (4), (5), and (8), which are a function of G_1, still hold.

Let us now evaluate the performance of R-PI controllers under uncertainty in the MFDs, i.e. the reality or plant MFD is different than the MFD to which the controller is designed for. The R-PI controller is designed according to the well-defined Yokohama MFD *without uncertainty*, however, it has been implemented to another two reality MFDs with variations of $+5\%$ and $+20\%$. The accumulation response results are shown in solid curves in Fig. 11. The results show that even though the R-PI controller is designed for a given well-defined MFD, the control is very robust for uncertainty in MFD, even with 20% deviation, the R-PI controller can bring the initial accumulation to the reference.

We also compare the performance of the previous R-PI controller with another R-PI controller that is designed taking into account the *MFD uncertainty* in the design process, i.e. the lower envelope has been set as the Yokohama MFD and the upper envelope has been set as the MFD with variation of $+20\%$. The comparison results are shown in Fig. 11, where the solid curves are the accumulation responses of the R-PI controller designed according to Yokohama MFD, and implemented for three different plant (reality) MFDs: Yokohama, deviations $+5\%$, and $+20\%$, and the cross marker points are the accumulation responses of the R-PI controller designed according to uncertainty up to 20% in MFD, and implemented for three different plant (reality) MFDs: Yokohama, deviations $+5\%$ and $+20\%$. The results show that the R-PI controllers have the same performance, as the accumulation responses for both controllers coincide. Note that one might conclude from this example that performance advantages are not gained by integrating the MFD uncertainty in the control design process. This conclusion is not correct, because the MFD uncertainty has been already taken into account in implicit way by considering the uncertainty in α. Since α can vary between 0 and 1, and it is multiplied by $G_1(\cdot)$, see (11), the uncertainty in α usually cover the uncertainty in $\alpha \cdot G_1(n)$ or $(1-\alpha)\cdot G_1(n)$ without considering the uncertainty in G_1. Note that this might not hold for extremum cases, e.g. α or $1-\alpha$ is close to 1, which will result in minor differences between both R-PI controllers. However, these cases are usually not physical.

In numerical example 5, the R-PI controller is examined for uncertainties in MFD, and errors in accumulation which are considered as plant output disturbances, see D_{out} in Fig. 2. Two cases are tested in Example 5: (5a) *biased* errors in MFD and accumulation, and (5b) *unbiased* errors in MFD and *biased* errors in accumulation. The biased errors in MFD can describe a well-defined MFD estimated with shifted errors, while the unbiased errors can describe an MFD with hysteresis loops that have been observed in the literature. In both cases, the biased errors in accumulation are tested for step shape errors, which are large errors compared with other shapes. The step shape error can describe e.g. occurrence of sensor structural failure or error in estimation because of weather conditions, and it results in overestimating or underestimating the number of vehicles in the region by the size of the step error. Although the probability of such errors to occur is low, considering step shape errors should cover many other types of error which are less effective.

In case (5a) a biased error in MFD is assumed, which is a deviation of 20% from the critical accumulation and the maximum trip completion flow of the Yokohama MFD as shown in Fig. 9, and different sizes of step error in accumulation 200—500 (veh) are imposed during the transient period at $t = 500$ (s) and the steady-state period at $t = 2000$ (s), which result in overestimating the number of vehicles in the region. The accumulations over time, the control input sequences, and the MFD evolution for the transient period are respectively shown in Fig. 12(a)–(c), while the results for the steady-state period are shown in Fig. 12(d)–(f). The results show that the R-PI controller can reject step errors as long as the steady-state necessary condition with output errors (34) holds. Therefore, the maximum step size that can be rejected is $d_{out,max} \approx 500$ (veh), which is calculated according to (34) with $A_{min} = -0.0084, B_{max} = -5, \widetilde{P}_{max} = 1$. This is numerically verified in Fig. 12(a) and (d), as the R-PI controller can reject step errors up to 400 (veh) during both steady-state and transient periods, while steady-state errors from reference occur for a step error with a size of 500 (veh). Clearly, the steady-state errors become larger as the step error size increases.

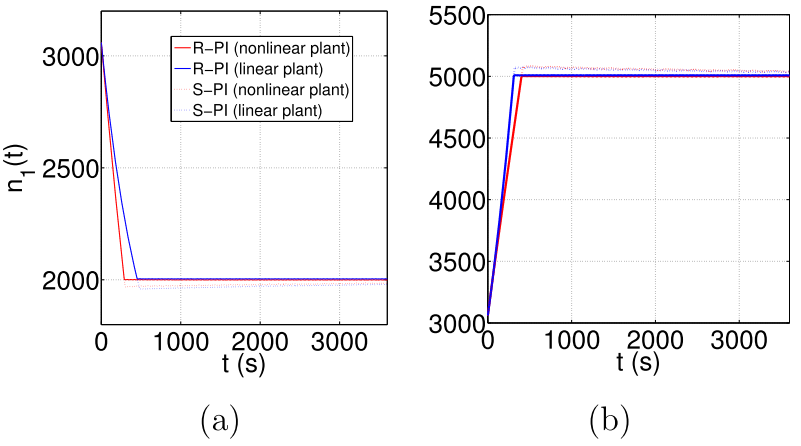

Fig. 8. Example 3: Accumulations vs. time for S-PI and R-PI controllers nearby the region of (a) uncongested and (b) congested set-points.

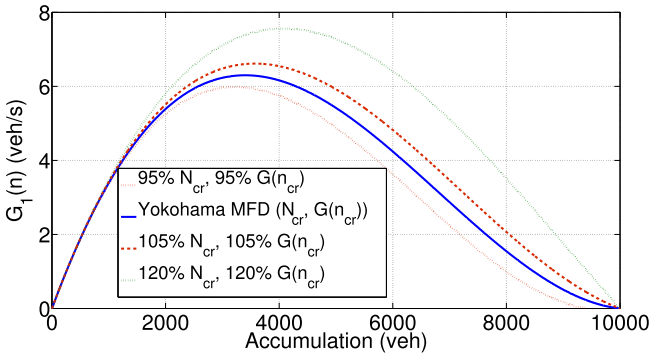

Fig. 9. Example 4: Yokohama MFD and another three variations of MFDs.

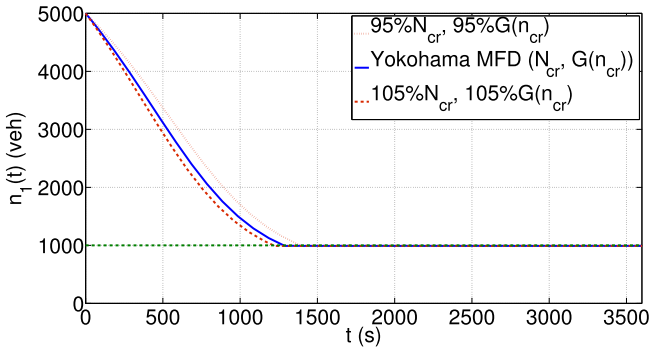

Fig. 10. Example 4: Accumulation responses to R-PI controllers designed according to different well-defined MFDs.

The R-PI controller is further tested for unbiased errors in MFD in case (5b). The MFD error, denoted by $\varepsilon(\cdot)$ (veh/s), is assumed to be uniformly distributed between lower and upper bounds of $n_1(t)$, as $\varepsilon(\tilde{n}_1(t)) \sim U(-\kappa \cdot \tilde{n}_1(t),\ \kappa \cdot \tilde{n}_1(t))$, and $\widetilde{G}_1(\tilde{n}_1(t)) = G_1(\tilde{n}_1(t)) + \varepsilon(\tilde{n}_1(t))$, where κ (1/s) is a parameter, $\tilde{n}_1(t)$ and $\widetilde{G}_1(\cdot)$ are respectively the accumulation and the MFD with errors. Note that the error in MFD increases with the accumulation in the region, as described e.g. in Geroliminis and Sun (2011b). The biased errors in accumulation are similar to case (5a). The R-PI controller is tested in case (5b) for different levels of error: (i) without any errors, (ii) error in accumulation with a step size of 300 (veh) and small errors ($\kappa = 0.2$ (1/s)) in MFD, (iii) error in accumulation with a step size of 300 (veh) and large errors ($\kappa = 0.6$ (1/s)) in MFD, and (iv) error in accumulation with a step size of 500 (veh) and large errors ($\kappa = 0.6$ (1/s)) in MFD. Note that (ii) and (iii) have the same size of the step error in accumulation but with different levels of error in MFD, while (iii) and (iv)

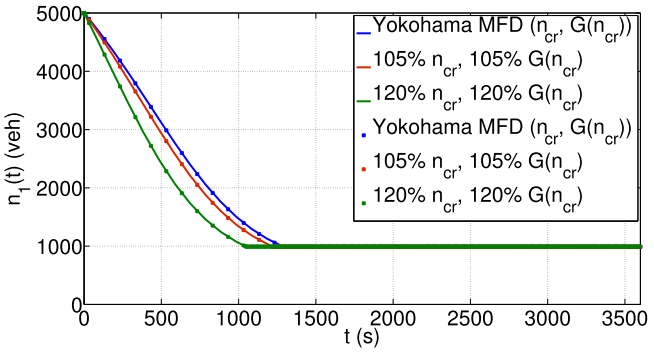

Fig. 11. Example 4: (a – solid curves) R-PI controller designed according to Yokohama MFD, and implemented for three different plant (reality) MFDs: Yokohama, deviations +5% and +20%, (b – cross marker points) R-PI controller designed according to uncertainty up to 20% in MFD, and implemented for three different plant (reality) MFDs: Yokohama, deviations +5% and +20%.

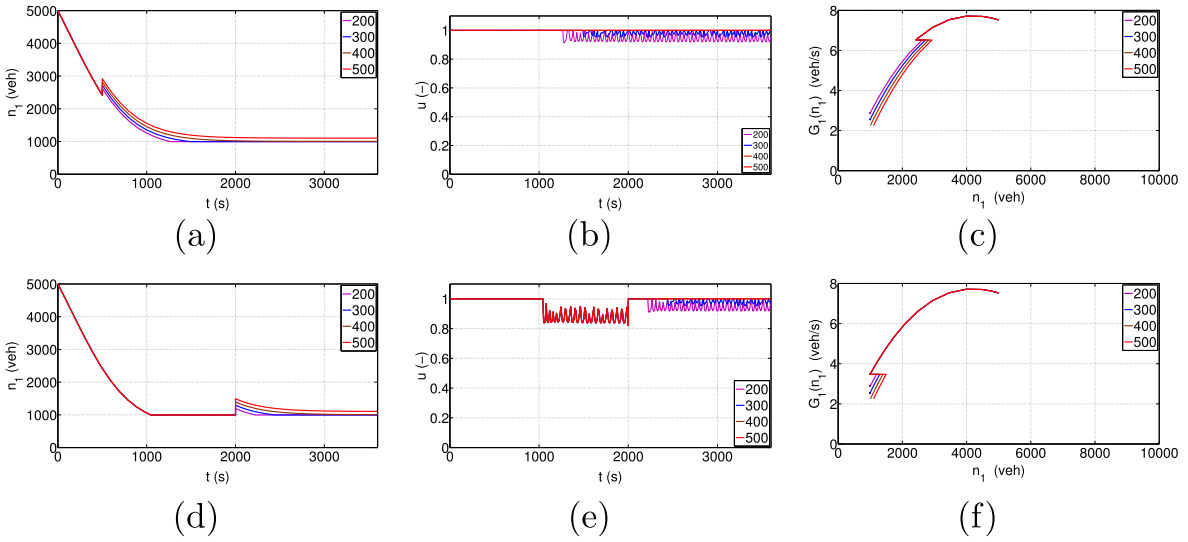

Fig. 12. Example 5a: A biased error of 20% in MFD and biased errors in accumulation 200—500 (veh) during the transient period at $t = 500$ (s): (a) accumulations over time, (b) control input sequences, and (c) MFD evolution, and during the steady-state period at $t = 2000$ (s): (d) accumulations over time, (e) control input sequences, and (f) MFD evolution.

have the same level of errors in MFD but with different sizes of step error. The accumulation, control input sequences, and MFD evolutions are respectively shown in Fig. 13(a)–(c). The results clearly show two time periods, before and after the step error at $t = 500$ (s) in Fig. 13(a), which corresponds to $n_1(500) = 3122$ (veh) in Fig. 13(c). It is shown in Fig. 13(c) that before the occurrence of the step error at $t = 500$ (s), the MFD evolution for (i) without any errors, plotted in black colour, is placed in the center of the MFD evolution for (ii), (iii), and (iv), plotted in blue, green, and red colours, respectively, where (iii) and (iv) have the same large errors and high-scattered points, and (ii) has smaller errors and low-scattered points. During $t > 500$, all curves are shifted to the left because of the biased errors in accumulation.

Comparing the accumulation results in Fig. 13(a) between (ii) and (iii), where both have the same step error size of 300 (veh) but with small errors in MFD for (ii) and large errors for (iii), show that the R-PI controller can reject increasing the MFD errors from small to large. On the other hand, increasing the error in accumulation from 300 in (iii) to 500 (veh) in (iv) while keeping the same large errors in MFD, the R-PI controller cannot reject the error as it exceeds the maximum disturbance value $d_{\text{out,max}}$. Similar to the results of case (5a), the results of case (5b) in Fig. 13(a) show that the R-PI controller has a good performance up to a step error size of 400 (veh) in accumulation. These results show that R-PI controller has stronger robustness against MFD errors than accumulation errors. This is correct since the error in MFD is treated within the uncertainty in the model parameters, α and $\widetilde{G}_1$, to which the R-PI controller has been designed for, while the error in accumulation is considered as an output error to which the R-PI controller can reject it as long as the constraints are not violated.

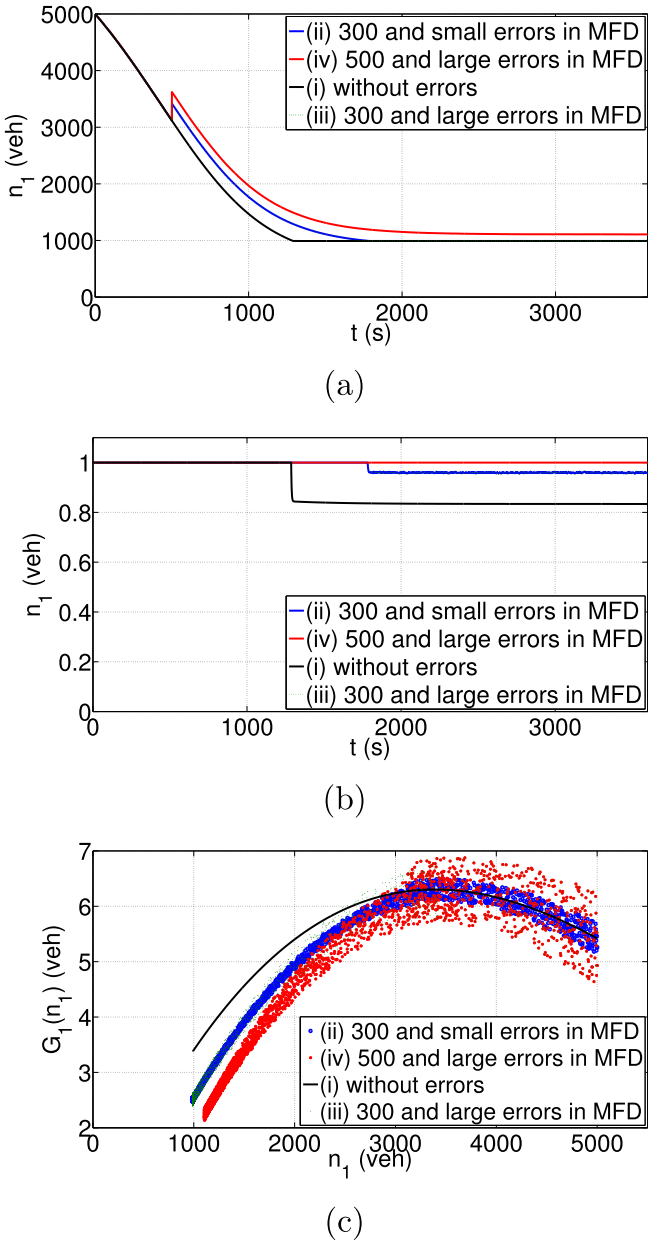

Fig. 13. Example 5b: Unbiased errors in MFD and biased errors in accumulation 200—500 (veh) during the transient period at $t = 500$ (s): (a) accumulations over time, (b) control input sequences, and (c) MFD evolution.

5. Conclusions and future work

A robust control design for a perimeter traffic flow at an urban region has been presented. First, the nonlinear vehicle-conservation model has been transformed to a linear model with MFD and parameter uncertainties, then the controller is designed by the linear model handling systematically the control constraint in the design process by utilizing a describing function, and implemented in both linear and nonlinear models. Analytical equations are derived for determining the robust PI controller gains K_P and K_I.

The results show that the derived linear model with parameter uncertainty can replace the original nonlinear model for modeling the traffic dynamics and for designing the robust perimeter controller, as long as the steady-state and transient necessary conditions hold. Moreover, the results demonstrate the importance of designing a robust controller, as comparison results between the S-PI and R-PI controllers show that the R-PI is superior for the numerical examples presented, since it can handle different cases and various situations, e.g. the difference between the S-PI and R-PI controllers is more apparent,

when the initial and final accumulations are far from each other, as the traffic dynamic (MFD shape) significantly changes moving from congested to uncongested or vice versa.

The S-PI controller performs well and satisfies the specifications given the design inputs. While its parameters should be tuned usually to adapt any changes in the inputs to which was designed for, the presented robust control design provides a fixed controller with K_I and K_P, which stabilizes the system and satisfies the specifications against all uncertainties in the model. Note that adjusting the gains in real time within an adaptive control approach would be another solution approach, however, other non-trivial tasks, e.g. guarantying stability or convergence to the reference accumulation, should be addressed. The R-PI controller was shown to be efficient for different congestion-level examples, as it is designed having the flexibility to bring initial accumulations to desired accumulations that are not necessary equal to the set-point. Moreover, the performance of the R-PI controller has been tested for different levels of demand, sizes and uncertainty in MFDs.

Two important issues should be considered towards implementing the R-PI controller in real networks. The first issue is how to actuate the control inputs of the R-PI controller by the signal timing plans operated by the traffic light signals located at the region border. A distributed robust control approach can shed more light towards this direction. The second issue is how to estimate the accumulation or number of vehicles (the state variable) with different sensing techniques of the network. Conceptually, the total number of vehicles inside the region might be approximated by considering a representative small area which is occupied with e.g. loop detectors sensors, that can estimate the number of vehicles in that area, and since the region is assumed to be homogeneous, the estimated number of vehicles in the area could be aggregated to the region level. Note that the numerical examples show that the R-PI controller is robust for overestimating or underestimating the number of vehicles up to an error level. However, a rigorous research should be conducted towards this direction, with the help of the works in Keyvan-Ekbatani et al. (2013), Leclercq et al. (2014) and Ortigosa et al. (2013), where the observability of the MFD with different sensing techniques have been studied.

The control approach based on the QFT, which is utilized in this paper to design a robust controller for an urban region, can be also applied to design robust controllers for a network with multiple regions. A future research direction might focus on extending the model for multiple urban regions. While analytical solutions and conditions were derived for the one urban region system, the mathematical derivation would be too tedious and not a trivial task for a network with multiple regions. However, the authors believe that such conditions will shed light in understanding and interpretation the numerical solutions that will be obtained for the multiple regions problem. Therefore, another future research direction might focus on deriving similar conditions to a system with only two urban regions.

A challenging control direction is how to derive the optimal accumulation references of a network with multiple regions, to which the controllers should regulate around or track them. Note that the accumulation references can be a priori given set points, or other desired constant accumulation points, or accumulation trajectories which might vary with time. The accumulation reference of the presented approach in this paper is assumed to be any desired constant accumulation, and the designed robust controller should regulate around it. In the case of multiple regions, it is clear that in some cases, e.g. when a network is heavily congested, the controllers might not succeed to regulate around all reference accumulation points, or sometimes the reference points should be changed during the control process. In principle, the robust R-PI controller developed for the one region system, which can be extended to a multiple region system, should also work if the reference points are being changed slower than the accumulation dynamics, but satisfying the control specifications are not guaranteed. A future research would be to develop perimeter controllers that aim at tracking accumulation references that vary with time.

Acknowledgments

This research was financially supported by the Technion. The research leading to these results has received funding from the European Union's – Seventh Framework Programme (FP7/2007–2013) under grant agreement n° 630690 – MC-SMART. The authors would like to thank Prof. Per-Olof Gutman from Technion for his suggestions and help with integrating the control constraint within the control loop. The authors would like to thank the anonymous reviewers for their valuable comments and suggestions to improve the quality of the paper.

Appendix A

This appendix presents the derivation of the steady-state values of $n_{11,ss}, n_{12,ss}, u_{ss}$. In steady-state it holds that the derivatives of the state variables $n_{11}(t)$ and $n_{12}(t)$ are equal to zero, i.e. $dn_{11}/dt = dn_{12}/dt = 0$. From (1) and (2), one gets

$$q_{11,ss} + (1 - u_{ss}) \cdot q_{21,ss} = \frac{n_{11,ss}}{n_{1,ss}} \cdot G_1(n_{1,ss}), \tag{A.1}$$

$$q_{12,ss} = \frac{n_{12,ss}}{n_{1,ss}} \cdot G_1(n_{1,ss}) \cdot u_{ss}. \tag{A.2}$$

One can eliminate $G_1(n_{1,ss})$ by dividing (A.1) by (A.2),

$$\frac{n_{11,ss}}{n_{12,ss}\cdot u_{ss}} = \frac{q_{11,ss} + (1-u_{ss})\cdot q_{21,ss}}{q_{12,ss}}, \tag{A.3}$$

and recalling that $n_{11,ss} + n_{12,ss} = n_{1,ss}$, one gets

$$n_{11,ss} = n_{1,ss}\cdot\left(1 - \frac{q_{12,ss}}{q_{11,ss} + q_{12,ss} + (1-u_{ss})\cdot q_{21,ss}}\right), \tag{A.4}$$

$$n_{12,ss} = n_{1,ss}\cdot\frac{q_{12,ss}}{q_{11,ss} + q_{12,ss} + (1-u_{ss})\cdot q_{21,ss}}. \tag{A.5}$$

Note that the values of $q_{11,ss}, q_{12,ss}, q_{21,ss}$, and $n_{1,ss}$ in (A.4) and (A.5) are assumed to be known in steady-state, while u_{ss} should be calculated. Multiplying (A.1) by u_{ss} and summing the result with (A.2), one gets the following

$$q_{21,ss}\cdot u_{ss}^2 - (q_{11,ss} + q_{21,ss} - G_1(n_{1,ss}))\cdot u_{ss} - q_{12,ss} = 0. \tag{A.6}$$

This equation is a quadratic equation that has only one admissible solution for u_{ss}.

Appendix B

This appendix provides a brief fundamental information about linearization of a nonlinear model and building-up a closed loop diagram. For more information, the reader can refer to Ogata (2010).

Let us consider a nonlinear system with uncertain parameter δ,

$$\frac{dx(t)}{dt} = F(x,u,\delta), \tag{B.1}$$

where $x \in \mathbb{R}$ is the state variable and $u(t) \in \mathbb{R}$ is the control variable. To obtain a linear model for the nonlinear model (B.1), it is assumed that the variable and control input derivate only slightly from an operation condition. Linearizing the nonlinear system model (B.1) around a given set-point $(\hat{x},\hat{u})$, one gets the following linear parameter-varying (LPV) model

$$\frac{d\Delta x(t)}{dt} = A(\delta)\cdot\Delta x(t) + B(\delta)\cdot\Delta u(t), \tag{B.2}$$

where $\Delta x(t) = x(t) - \hat{x}$ and $\Delta u(t) = u(t) - \hat{u}$, and

$$A(\delta) = \left.\frac{\partial F}{\partial x}\right|_{x=\hat{x},u=\hat{u}} \quad \text{and} \quad B(\delta) = \left.\frac{\partial F}{\partial u}\right|_{x=\hat{x},u=\hat{u}}. \tag{B.3}$$

The LPV model (B.2) with uncertain parameter δ approximates the original nonlinear system (B.1) near the set-point $(\hat{x},\hat{u})$. The Laplace transformation is applied to the linear model (B.2), which is transformed to the frequency domain as follows

$$\Delta X = P\cdot\Delta U = \frac{B(\delta)}{s - A(\delta)}\cdot\Delta U. \tag{B.4}$$

Then, the LPV model (B.4) is chosen as the plant, and it is integrated in a closed loop diagram as shown in Fig. B.1, where ΔX_{ref} is the state reference, G is the controller, $P(\delta)$ in the uncertain plant, ΔU is the control input, D_{in} and D_{out} are respectively the the plant input and output disturbances. The closed-loop transfer function, which relates the state reference ΔX_{ref}, the output disturbance D_{out}, and the input disturbance D_{in} to the output ΔX, is calculated as follows

$$\Delta X = \mathcal{CL}_{\Delta X_{ref},\Delta X}\cdot\Delta X_{ref} + \mathcal{CL}_{D_{out},\Delta X}\cdot D_{out} + \mathcal{CL}_{D_{in},\Delta X}\cdot D_{in}, \tag{B.5}$$

where the closed loop transfer functions from state reference to output, $\mathcal{CL}_{\Delta X_{ref},\Delta X}$, plant input disturbance to output, $\mathcal{CL}_{D_{in},\Delta X}$, and plant output disturbance to output $\mathcal{CL}_{D_{out},\Delta X}$, are respectively calculated as follows:

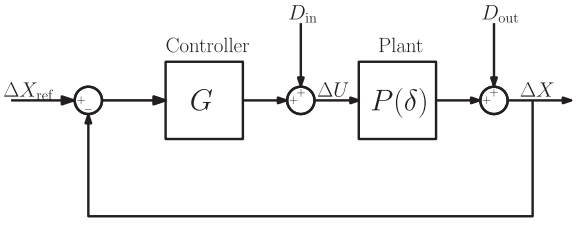

Fig. B.1. A closed-loop block diagram for uncertain plant $P(\delta)$.

$$\mathcal{CL}_{\Delta X_{\mathrm{ref}},\Delta X} = \frac{GP}{1+GP}, \tag{B.6}$$

$$\mathcal{CL}_{D_{\mathrm{in}},\Delta X} = \frac{P}{1+GP}, \tag{B.7}$$

$$\mathcal{CL}_{D_{\mathrm{out}},\Delta X} = \frac{1}{1+GP}. \tag{B.8}$$

References

Aboudolas, K., Geroliminis, N., 2013. Perimeter and boundary flow control in multi-reservoir heterogeneous networks. Transportation Research Part B 55, 265–281.

Buisson, C., Ladier, C., 2009. Exploring the impact of homogeneity of traffic measurements on the existence of macroscopic fundamental diagrams. Transportation Research Record 2124, 127–136.

Camacho, E.F., Bordons, C., 1999. Model Predictive Control. Springer-Verlag, Berlin, Germany.

Daganzo, C.F., 2007. Urban gridlock: macroscopic modeling and mitigation approaches. Transportation Research Part B 41 (1), 49–62.

Daganzo, C.F., Gayah, V.V., Gonzales, E.J., 2011. Macroscopic relations of urban traffic variables: bifurcations, multivaluedness and instability. Transportation Research Part B 45 (1), 278–288.

Gelb, A., Velde, W.V., 1968. Multiple-Input Describing Functions and Nonlinear System Design. McGraw Hill.

Geroliminis, N., Boyacı, B., 2012. The effect of variability of urban systems characteristics in the network capacity. Transportation Research Part B 46 (10), 1607–1623.

Geroliminis, N., Daganzo, C.F., 2008. Existence of urban-scale macroscopic fundamental diagrams: some experimental findings. Transportation Research Part B 42 (9), 759–770.

Geroliminis, N., Haddad, J., Ramezani, M., 2013. Optimal perimeter control for two urban regions with macroscopic fundamental diagrams: a model predictive approach. IEEE Transactions on Intelligent Transportation Systems 14 (1), 348–359.

Geroliminis, N., Sun, J., 2011a. Hysteresis phenomena of a macroscopic fundamental diagram in freeway networks. Transportation Research Part A 45 (9), 966–979.

Geroliminis, N., Sun, J., 2011b. Properties of a well-defined macroscopic fundamental diagram for urban traffic. Transportation Research Part B 45 (3), 605–617.

Godfrey, J.W., 1969. The mechanism of a road network. Traffic Engineering and Control 11 (7), 323–327.

Haddad, J., Geroliminis, N., 2012. On the stability of traffic perimeter control in two-region urban cities. Transportation Research Part B 46 (1), 1159–1176.

Haddad, J., Ramezani, M., Geroliminis, N., 2013. Cooperative traffic control of a mixed network with two urban regions and a freeway. Transportation Research Part B 54, 17–36.

Hajiahmadi, M., Haddad, J., Schutter, B.D., Geroliminis, N., 2013. Optimal hybrid macroscopic traffic control for urban regions: Perimeter and switching signal plans controllers. In: European Control Conference, July 17–19, 2013, 13.

Houpis, C.H., Rasmussen, S.J., Garcia-Sanz, M., 2006. Quantitative Feedback Theory: Fundamentals and Applications. CRC Press, Taylor & Francis Group.

Ji, Y., Daamen, W., Hoogendoorn, S., Hoogendoorn-Lanser, S., Qian, X., 2010. Macroscopic fundamental diagram: Investigating its shape using simulation data. Transportation Research Record 2161, 42–48.

Ji, Y., Geroliminis, N., 2012. On the spatial partitioning of urban transportation networks. Transportation Research Part B 46 (10), 1639–1656.

Keyvan-Ekbatani, M., Kouvelas, A., Papamichail, I., Papageorgiou, M., 2012. Exploiting the fundamental diagram of urban networks for feedback-based gating. Transportation Research Part B 46 (10), 1393–1403.

Keyvan-Ekbatani, M., Papageorgiou, M., Papamichail, I., 2013. Urban congestion gating control based on reduced operational network fundamental diagrams. Transportation Research Part C, 74–87.

Knoop, V., Hoogendoorn, S., van Lint, H., 2013. The impact of traffic dynamics on the macroscopic fundamental diagram. In: 92nd Annual Meeting of Transportation Research Board, Washington, DC, USA.

Knoop, V.L., Hoogendoorn, S.P., Van Lint, J.W.C., 2012. Routing strategies based on the macroscopic fundamental diagram. Transportation Research Record 2315, 1–10.

Leclercq, L., Chiabaut, N., Trinquier, B., 2014. Macroscopic fundamental diagrams: a cross-comparison of estimation methods. Transportation Research Part B, 1–12.

Mahmassani, H., Williams, J., Herman, R., 1987. Performance of urban traffic networks. In: Gartner, N., Wilson, N. (Eds.), Proceedings of the 10th International Symposium on Transportation and Traffic Theory. Elsevier, Amsterdam, The Netherlands.

Mahmassani, H.S., Saberi, M., Zockaie, A.K., 2013. Network gridlock: Theory, characteristics, and dynamic. In: Procedia - Social and Behavioral Sciences, vol. 80, pp. 79–98, doi:10.1016/j.sbspro.2013.05.007. 20th International Symposium on Transportation and Traffic Theory.

Mazloumian, A., Geroliminis, N., Helbing, D., 2010. The spatial variability of vehicle densities as determinant of urban network capacity. Philosophical Transactions of the Royal Society A: Mathematical, Physical and Engineering Sciences 368 (1928), 4627–4647.

Ogata, K., 2010. Modern Control Engineering. Prentice Hall.

Olszewski, P., Fan, H.S.L., Tan, Y.-W., 1995. Area-wide traffic speed-flow model for the Singapore CBD. Transportation Research Part A 29A (4), 273–281.

Ortigosa, J., Menendez, M., Tapia, H., 2013. Study on the number and location of measurement points for an MFD perimeter control scheme: a case study of Zurich. EURO Journal on Transportation and Logistics. http://dx.doi.org/10.1007/s13676-013-0034-0.

Ramezani, M., Haddad, J., Geroliminis, N., 2013. Integrating the dynamics of heterogeneity in aggregated network modeling and control. In: Transportation Research Board Annual Meeting. No. 14-0710, Washington, DC

Saberi, M., Mahmassani, H., 2012. Exploring properties of network-wide flow-density relations in a freeway network. In: Transportation Research Board 91st Annual Meeting. Washington, DC.

Zhang, L., Garoni, T., de Gier, J., 2013. A comparative study of macroscopic fundamental diagrams of arterial road networks governed by adaptive traffic signal systems. Transportation Research Part B 49, 1–23.